SYNTHESIS, CHARACTERIZATION OF MAGNETIC NANOPARTICLES BASED ON $Mn_xFe_{3-x}O_4$ SPINEL BY MICRO-EMULSION BY AND THEIR ADSRPTION CAPACITY FOR As (V) IN SOLUTION

Received: *21-05-2025*

Vu The Ninh*, Nguyen Viet Dung, Ngo Huy Khoa

[1]*Institute of Materials Science, Vietnam Academy of Science and Technology*
**Email: ninhvt@ims.vast.ac.vn*

TÓM TẮT

XÁC ĐỊNH CÁC ĐẶC TRƯNG CỦA NANO OXIT TỪ TÍNH SPINEN MnxFe3-xO4 ĐƯỢC CHẾ TẠO BẰNG PHƯƠNG PHÁP VI NHŨ TƯƠNG VÀ ĐÁNH GIÁ KHẢ NĂNG HẤP PHỤ As(V) TRONG DUNG DỊCH

Đơn pha tinh thể của spinel $Mn_xFe_{3-x}O_4$ được chế tạo bằng phương pháp đồng kết tủa trong pha vi nhũ tương. Các đặc trưng tính chất của vật liệu đã được xác định. Đặc trưng tinh thể bằng phương pháp Nhiễu xạ tia X (XRD), hình thái học bề mặt được xác định bằng Kính hiển vi điện tử quét (SEM) và diện tích bề mặt riêng được xác định bằng phương pháp hấp phụ và giải hấp nitơ Brunaure-Emmet-Teller (BET), tính chất từ của mẫu vật liệu được xác định theo phương pháp Từ kế lấy mẫu rung (VSM). Kết quả cho thấy đơn pha tinh thể $Mn_xFe_{3-x}O_4$ ($0 \le x \le 0,9$) được hình thành do sự thay thế Fe(II) bằng Mn(II) trong mạng tinh thể Fe_3O_4 và tinh thể spinel pha đơn được hình thành trong phạm vi kích thước 4,7 - 9,8nm, diện tích bề mặt riêng trong phạm vi 134 - 204$m^2.g^{-1}$, độ từ hóa bão hòa đạt trong phạm vi 14 - 32$emu.g^{-1}$. Khả năng hấp phụ As(V) tốt nhất trên mẫu thay thế có công thức $Mn_{0,3}Fe_{2,7}O_4$ đạt tới 178 mgAs(V)/g.

Từ khóa: *Spinen $Mn_xFe_{3-x}O_4$, tính chất từ, hấp phụ As(V), kích thước nano.*

1. INTRODUCTION

The applications of spinel oxide materials in general and ferrite spinel oxide in particular are very wide and multidisciplinary. They have been used as magnetic materials [1, 2], as adsorbents for removing heavy metals [3, 4] and dyes [5, 6] from water and wastewater, or as catalysts and photocatalysts for removing various pollutants [7, 8]. In addition, they could be used as contrast agents [9], hyperthermia [10, 11], drug delivery and release [12, 13], as sensors/biosensors in biotechnology and medical applications, in electronic devices, microwave devices, recording devices, etc. [14-16].

Ferrite spinel oxide catalytic and adsorbent materials could directly access the polluted object, so the treatment efficiency was high, the treated material could be reused by collection, purified from the environment by external magnetic force. Therefore, these magnetic nanoparticles had the greatest impact in environmental treatment, through the removal of pollutants from groundwater and marine environments or by improving the quality of domestic water. The process of water pollution was complicated due to agents: organic, heavy metals, antibiotic residues, pesticides... related to industrial production and urbanization [17-19]. In particular, arsenic pollution in groundwater and surface water was quite common in the world. Regular exposure to water sources contaminated with arsenic at concentrations >50 µg.L-1 could cause serious health problems related to skin, cardiovascular, hematological, and respiratory diseases.

In water, arsenic existed stably at high concentrations under different conditions of oxidation-reduction potential and pH, so the removal of arsenic from water sources was much more difficult than other polluting elements [20-22]. Adsorbed arsenic had been shown to form complexes (monodentate, didentate) with hydroxyl (-OH) functional groups on materials such as MnO_2, Mn_2O_3, Fe_2O_3, Fe_3O_4 compounds, or/and precipitate with dissociable compounds such as FeOOH, $Fe(OH)_3$, $La(OH)_3$, $La_2(CO_3)_3$ [23-28].

On the other hand, spinel ferrite oxide could be prepared by various methods and the original structure was not limited in its ability to be modified, so scientists were interested in preparing it for many different applications. For example, the compound Fe_3O_4 could be modified by replacing Fe(II) with transition metals as shown in the formula $Fe_{1-x}A_xFe_2O_4$ (A = Mn, Cu, Co, Ni, Zn, Mg) to form compounds with chemical stability, while improving their magnetism as well as enhancing their adsorption capacity compared to the original compound [29-32]. The results showed that replacing Fe(II) with Mn(II) in the formula $Fe_{1-x}Mn_xFe_2O_4$ increased the adsorption efficiency of As, methyl orange, Congo red and some other heavy metals [33]. If Fe(II) was completely replaced, the removal efficiency of Cr(VI) increased in the order $NiFe_2O_4 < CuFe_2O_4 < ZnFe_2O_4 < MgFe_2O_4 < MnFe_2O_4$ [34]…

In the previous study [35], the successful fabrication of spinel to replace $Mn_{0.5}Fe_{2.5}O_4$ by co-precipitation method in microemulsion phase was reported. Continuing, in this paper, the fabrication results of spinel system to replace $Mn_xFe_{3-x}O_4$ ($0 \leq x \leq 1$), as well as the characteristics and adsorption capacity to remove As(V) from solution are presented.

2. EXPERIMANTAL

2.1. Chemicals

All reagents were at analytical grade and used as received without further purifi cation. $FeCl_3.6H_2O$, $FeCl_2.4H_2O$, $MnCl_2.4H_2O$, NaOH, HCl and Dietylen glycol dietyl ete ($C_8H_{18}O_3$, DGDE), Na_3AsO_4, acetone were purchased from Sigma-Aldrich and Merck. Deionized water was used for all experiments.

2.2. Synthesis of $Mn_xFe_{3-x}O_4$ spinel

Firstly, prepared a solution mixture of chloride salts of the cations Fe^{2+}, Mn^{2+}, Fe^{3+}, with the following conditions: The ratio of $Fe^{2+}/Mn^{2+}/Fe^{3+}$ was taken so as to form $Mn_xFe_{3-x}O_4$, where x had the values 0; 0.1; 0.3; 0.5; 0.7; 0.9; 1, solution pH value = 2 - 3, the specified temperature, was called solution A. Then, while stirring an exact volume of DGDE solvent, dripping all solution A to the DGDE solvent to form the micro-emulsion phase with milky yellow color, was called solution B. Next, the co-precipitation was carried out by dripping the 1,5 M NaOH solution into solution B until the medium stabilizes with pH value = 9-10 (proceed on the mechanical stirrer). Finally, separated the precipitate, the decouldter wash several times with water with external magnetic field, washed the centrifuge once with water, two times with acetone and the drying at a suitable temperature to obtain nano-ferrites. In the coprecipitation reaction, solvent/water volume ratio was keep at 1/3 (O/W), ion metal molar concentration in solution (C_M) 0,25M, coprecipitation process temperature (initial temperature-T_R) at 30^{o}C. The co-precipitated sample was dried at 80°C for 5 hours before receiving the XRD patterns. The average crystal phase size of the ferrite spinel is determined by semi-empirical equation Scherrer (d, nm).

2.3. Characterization methods

The products obtained during different stages were characterized by X-ray diffraction (XRD) using a D8 ADVANCE diffractometer (Bruker, Germany) with CuKα radiation (λ = 1.5046 Å) in the range of 2θ = 20° - 80°. The average crystal size of the material was determined by the Scherrer semi-empirical equation as follows:

$$X\,(Å) = \frac{B * \lambda}{\beta * \cos\theta}$$

where, X was the average crystal particle size, θ (degree) corresponding to angle sweeping at the maximum peak, β was width of the half maximum peak (radian), B is Scherrer constant (≈ 0.9).

The micro-structure image and elemental composition of sample the sample was evaluated by scouldning electron microscopy combined energy dispersive X-ray spectroscopy (SEM-EDX) using a S4800 microscope (Hitachi, Japan). The specific surface area was determined by the Brunauer-Emmett-Teller (BET) method by liquid N_2 adsorption at 77K on TriStar II Plus 2.03 analyzer (Micromeritics, USA). Vibration sample magnetometer (VSM) measured on measuring equipment at Institute of Materials Science, Vietnam Academy of Science and Technology (IMS-VAST, Vietnam).

2.4. Determine the maximum adsorption capacity

The saturated adsorption capacity (Q_{bh}, $mg.g^{-1}$) of As(V) of the material was determined by conducting an adsorption experiment between 100 mL of solution with different initial concentrations of As(V) (C_i, $mg.L^{-1}$) with 0.05 g of spinel oxides. When the adsorption equilibrium, collect the solution to determine the remaining concentration of As(V) (C_f, $mg.L^{-1)}$. The saturated adsorption capacity was calculated by the formula: $Q_{bh} = 2*(C_i-C_f)$.

The maximum adsorption capacity of spinel oxides (Q_{max}, $mg.g^{-1}$) for As(V) was determined according to Langmuir isotherm adsorption model. Represent the experimental points (Q_{bh}, C_f) determined on the graph showing the dependence of Q_{bh} on C_f and regress those experimental values by using specialized calculation software Table Curve. 2D 5.01 to obtain the maximum adsorption capacity of the spinel oxides for As(V).

2.4. Methods of elemental analysis

Determination of ionic content of elements As(V) Fe, Mn and other elements in solution by atomic absorption method (AAS) on instrument 200 Series AA (Agilent, USA).

3. RESULT AND DISCUSSION

3.1. Determination of spinel $Mn_xFe_{3-x}O_4$ characteristics

3.1.1. Crystalline phase characteristics of spinel $Mn_xFe_{3-x}O_4$

The results of the investigation of the influence of the x-substitution component ($0 \le x \le 1$) on the formation of spinel oxide crystal phase according to the formula $Mn_xFe_{3-x}O_4$ were shown in the XRD diagram in Figure 1. The results in Figure 1 showed that, except for the sample with the x-substitution component being amorphous corresponding to the desire to replace Fe(II) with Mn(II) to form spinel oxide $Mn_xFe_{3-x}O_4$, all the remaining samples suggested the appearance of diffraction lines characteristic of the formation of spinel ferrite crystal phase.

Table 1. Average crystallite size of spinel $Mn_xFe_{3-x}O_4$

x	0	0,1	0,3	0,5	0,7	0,9	1,0
$d_{spinel\ ferit}$, nm	6,7	4,7	6,3	6,7	7,8	9,8	VĐH

For the samples forming crystalline phase, the XRD diagram also observed the shift of the scouldning angle at the maximum diffraction peak shifting from 35.371o to 35.041o when the x-substitution content in the $Mn_xFe_{3-x}O_4$ crystal phase was from 0 to 0.9. This demonstrates the complete substitution of Fe(II) by Mn(II) in each substitution component. In other words, a completely substituted solid solution $Mn_xFe_{3-x}O_4$ ($0 \leq x \leq 0.9$) was formed between the two spinel oxide phases $FeFe_2O_4$ and $MnFe_2O_4$.

However, under similar synthesis conditions, when Fe(II) was completely replaced by Mn(II), the $MnFe_2O_4$ crystal phase could not be formed. This showed that the crystallization of the spinel phase $Mn_xFe_{3-x}O_4$ occurs more easily in the presence of Fe(II) and the formation of the $MnFe_2O_4$ crystal phase had to be carried out under more stringent conditions. On the other hand, the results of calculating the average crystal phase size of spinel oxide $Mn_xFe_{3-x}O_4$ using the semi-empirical sherrer equation were shown in Table 1. The results showed that the crystal phase size decreased sharply when Fe(II) was replaced by 10% Mn, then increased slightly, and the crystal size increased significouldtly when x > 0.5.

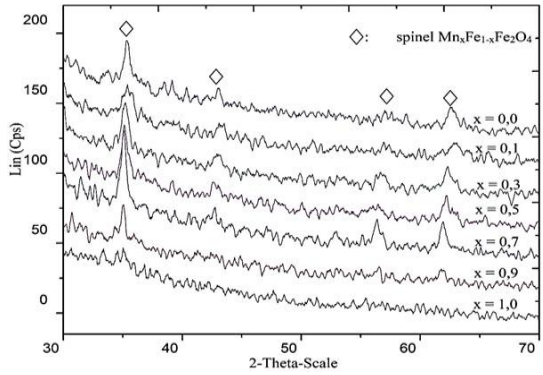

Figure 1. XRD patterns of spinel $Mn_xFe_{3-x}O_4$ samples

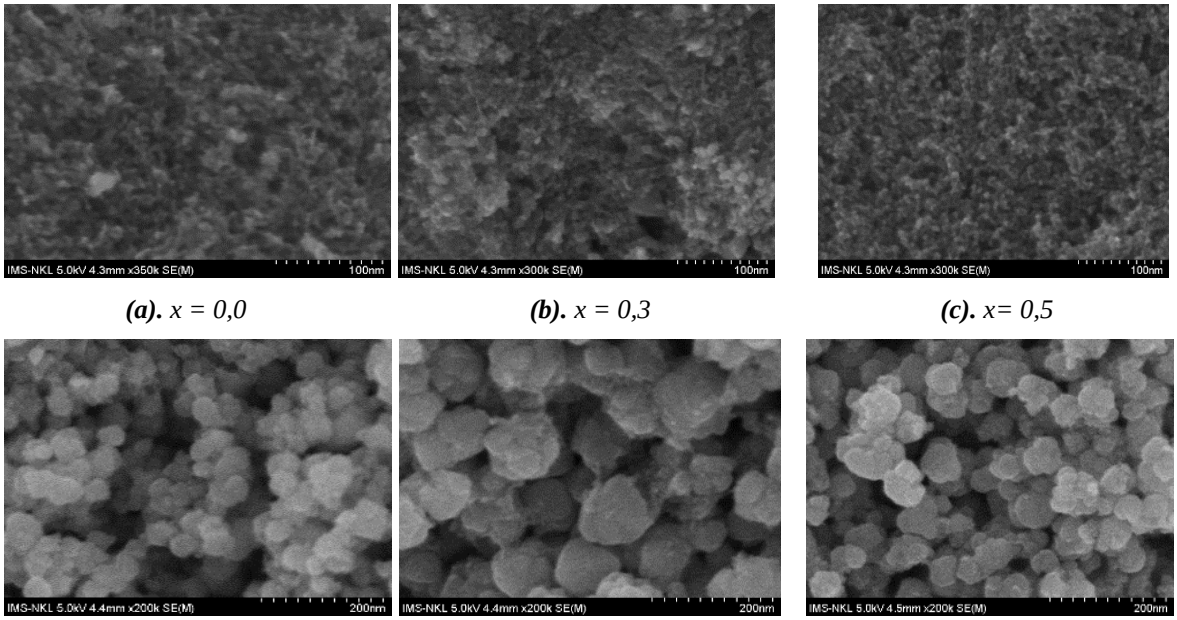

(a). *x = 0,0* ***(b).*** *x = 0,3* ***(c).*** *x= 0,5*

(d). *x = 0,7* ***(e).*** *x = 0,9* ***(f).*** *x = 1,0*

Figure 2(a-f). SEM images of spinel $Mn_xFe_{3-x}O_4$ samples

3.1.2. Morphological characteristics and surface area of spinel $Mn_xFe_{3-x}O_4$

The results of some characteristics of the surface area of the spinel oxide samples $Mn_xFe_{3-x}O_4$ ($0 \leq x \leq 1$) fabricated at

optimal conditions were shown in Table 2. The results in Table 2 showed that all the spinel oxide samples $Mn_xFe_{3-x}O_4$ ($0 \leq x \leq 1$) fabricated have very high surface areas reaching from 134 $m^2.g^{-1}$ - 204 $m^2.g^{-1}$.

When Mn was present, the pore size was significantly reduced and divided into two groups: (i). The first group of spinel oxides $Mn_xFe_{3-x}O_4$ with $0.1 \leq x \leq 0.5$, the formed particles had crystal size correlated with pore size, the pore volume was slightly reduced compared to the Fe_3O_4 sample (0.29 $cm^3.g^{-1}$) and did not change much between samples from 0.23 $cm^3.g^{-1}$ to 0.24 $cm^3.g^{-1}$, so the surface area of the sample was relatively high, reaching 193 $m^2.g^{-1}$ to 204 $m^2.g^{-1}$. When observed on the SEM image in Figure 2(a,b,c), it also showed that the samples had quite uniform sizes, good dispersion, size < 10 nm; (ii). In the second group, the spinel oxides $Mn_xFe_{3-x}O_4$ with $0.5 < x \leq 0.9$, the pore size did not change much, but the pore volume decreased significantly to 0.15 $cm_3.g^{-1}$ to 0.17 $cm^3.g^{-1}$ and the specific surface area decreased to 134 $m^2.g^{-1}$ to 160 $m^2.g^{-1}$. Similarly, when observing the surface morphology of these samples on the SEM images in Figure 2(d, e), it could be seen that the formed particles have the phenomenon of clustering into large clusters of particles with an average diameter of ~ 50 nm. However, the average pore size on these samples was determined to be relatively small, did not change much, and the specific surface area of the samples decreased but still reached a fairly high value. This result, possibly due to the formation of $Mn_xFe_{3-x}O_4$ solid solution at this Mn content, changed the crystal nature towards clustering.

In the case of spinel oxide sample $Mn_xFe_{3-x}O_4$ with x = 1 corresponding to $MnFe_2O_4$ compound, due to non-crystallization, there was no data on the average crystal phase size, but the sample had small pore diameter, large pore volume (0.24 $cm^3.g^{-1}$) and specific surface area of 203 $m^2.g^{-1}$, relatively large grain size ~50 nm when observed on SEM image in Figure 2(f).

Table 2. BET surface area characteristics of spinel $Mn_xFe_{3-x}O_4$ oxides

Parameters	Spinel $Mn_xFe_{3-x}O_4$ oxides						
	0,0	0,1	0,3	0,5	0,7	0,9	1,0
S_{BET}, m^2/g	176	204	202	193	134	160	203
V_{pore}, m^3/g	0,29	0,24	0,23	0,24	0,15	0,17	0,24
D_{pore}, nm	6,1	4,8	4,8	4,9	5,0	4,5	5,0

3.1.3. Magnetic characteristics of spinel $Mn_xFe_{3-x}O_4$

The VSM measurement results of the spinel oxide sample Fe_3O_4 corresponding to x = 0 were determined in Figure 3. The results showed that this was a superparamagnetic sample with a saturation magnetization of about 32 emu.g^{-1}. Similarly, the saturation magnetization of other spinel samples was also determined, the results were shown in Table 3. The spinel samples $Mn_xFe_{3-x}O_4$ with nano size had a saturation magnetization in the range of 13.6 emu.g^{-1} to 31 emu.g^{-1}, which was much lower than that of the bulk samples (80 emu.g^{-1} - 90 emu.g^{-1}, respectively).

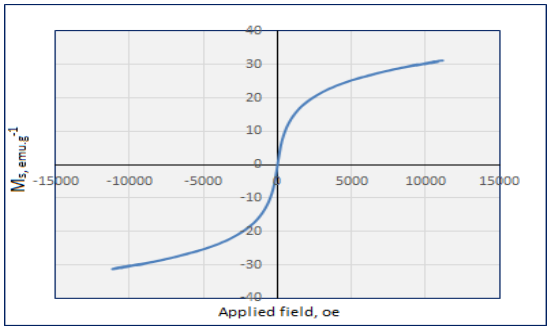

Figure 3. Magnetization curve of spinel Fe_3O_4 sample

In particular, the magnetic saturation of the x = 1 sample corresponding to $MnFe_2O_4$ is 13.6 emu.g^{-1}, which was much lower than that of the other samples. This was a set of samples that are considered to be quite similar in terms of surface morphology and grain size as determined in Table 3 and Figure 2. The only difference of the $MnFe_2O_4$ spinel was that the sample was in an amorphous aggregate state, which reduced the saturation magnetization of sample to low level.

Table 3. Saturation magnetization of the $Mn_xFe_{3-x}O_4$ spinel

X values	0,0	0,1	0,3	0,5	0,7	0,9	1,0
Ms, emu.g^{-1}	31	26	28	27	32	24	13,6

3.2. As(V) adsorption capacity of spinel $Mn_xFe_{3-x}O_4$

3.2.1. Effect of substitution composition of spinel $Mn_xFe_{3-x}O_4$ oxide

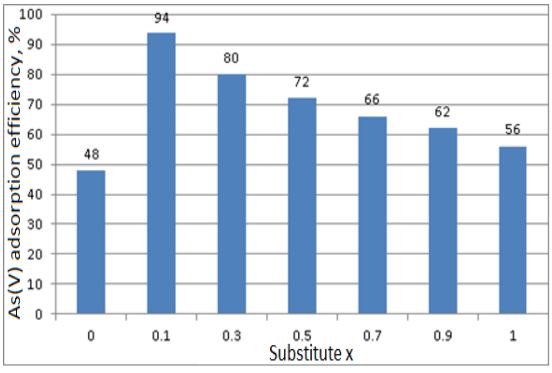

Figure 4. As(V) adsorption efficiency on spinel $Mn_xFe_{3-x}O_4$ oxide

The effect of the x component in spinel oxide $Mn_xFe_{3-x}O_4$ on As(V) adsorption efficiency was shown in Figure 4. The results in Figure 4 show that, when modified with Mn, spinel oxides $Mn_xFe_{3-x}O_4$ have a higher As(V) adsorption capacity than the original Fe_3O_4. From the As(V) adsorption efficiency on spinel $Mn_xFe_{3-x}O_4$, it was also seen that the effect increases strongly on the spinel sample $Mn_{0.1}Fe_{2.9}O_4$ and gradually decreases when the content of Mn substitution increases.

3.2.2. As(V) maximum adsorption capacity on spinel $Mn_{0.1}Fe_{2.9}O_3$ oxide

The Langmuir adsorption isotherm for As(V) on spinel $Mn_{0.1}Fe_{2.9}O_4$ material was shown in Figure 5. The results showed that the maximum adsorption capacity of As(V) on spinel $Mn_{0.1}Fe_{2.9}O_4$ material was 178 mg.g^{-1} with a regression coefficient of 99.9%.

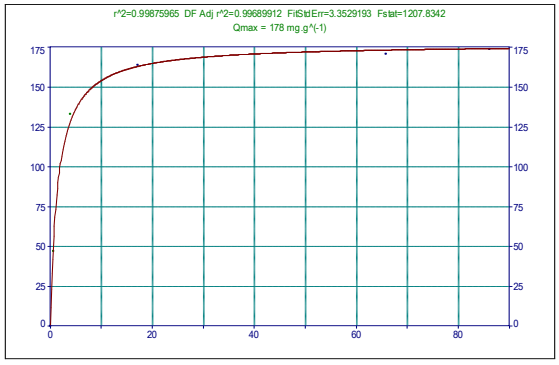

Figure 5. Langmuir adsorption isotherm for As(V) on spinel $Mn_{0.1}Fe_{2.9}O_3$ oxide

4. CONCLUSION

The product spinel $Mn_xFe_{3-x}O_4$ oxides ($0 \le x \le 1$) prepared under optimal conditions had the following characteristics:

+ A single phase of solid solution crystal completely replacing spinel oxide $Mn_xFe_{3-x}O_4$ ($0 \le x \le 0.9$) was formed. The average crystal size of spinel oxide $Mn_xFe_{3-x}O_4$ ($0 \le x \le 0.9$) decreased and depended on the substitution content x with a value in the range of 5 nm to 10 nm; The surface area of spinel oxide $Mn_xFe_{3-x}O_4$ ($0 \le x \le 0.9$) increased and depended on x with a value of about 130 m^2.g^{-1} to 200 m^2.g^{-1}, finally the saturation magnetization of these alternative samples was in the range of 24 emu.g^{-1} to 32 emu.g^{-1};

+ Under similar conditions, single-phase crystal of spinel oxide $MnFe_2O_4$ had not been formed. The amorphous compound of ferrite manganese oxide was $MnFe_2O_4$ with a surface area of 203 $m^2.g^{-1}$, the saturation magnetization reaches 12.6 $emu.g^{-1}$.

The adsorption capacity of As(V) on the prepared spinel oxide nano system $Mn_xFe_{3-x}O_4$ was determined: The spinel oxide compounds $Mn_xFe_{3-x}O_4$ had good adsorption capacity for As(V), the adsorption efficiency was highest on spinel $Mn_{0.1}Fe_{2.9}O_4$ oxide; The maximum As(V) adsorption capacity calculated according to the Langmuir adsorption isotherm model of spinel $Mn_{0.1}Fe_{2.9}O_4$ oxide was 178 $mg.g^{-1}$.

Acknowledgments

This research is funded by Nippon Sheet Glass Foundation for Materials Science and Engineering under grant number NSG Foundation 10.

Declaration: The authors declare that this is the authors' work and this content has not been submitted to any journal.

REFERENCES

[1]. J. Li, H. Yuan, G. Li, Y. Liu, J. Leng, (2010). Cation distribution dependence of magnetic properties of solgel prepared $MnFe_2O_4$ spinel ferrite nanoparticles. *Magn. Magn. Mater.*, **322(21)**, 3396-3400.

[2]. R. Raeisi Shahraki, M. Ebrahimi, S.A. Seyyed Ebrahimi, S.M. Masoudpanah, (2012). Structural characterization and magnetic properties of superparamagnetic zinc ferrite nanoparticles synthesized by the coprecipitation method. *Magn. Magn. Mater.*, **324(22)**, 3762-3765.

[3]. S. Zhang, H. Niu, Y. Cai, X. Zhao, Y. Shi, (2010). Arsenite and arsenate adsorption on coprecipitated bimetal oxide magnetic nanomaterials: $MnFe_2O_4$ and $CoFe_2O_4$. *Chem. Eng. J.*, **158(3)**, 599-607.

[4]. B.Y. Song, Y. Eom, T.G. Lee, (2011). Removal and recovery of mercury from aqueous solution using magnetic silica nanocomposites. *Appl. Surf. Sci.*, **257(10)**, 4754-4759.

[5]. W. Konicki, D. Sibera, E. Mijowska, Z. Lendzion-Bielun, U. Narkiewicz, (2013). Equilibrium and kinetic studies on acid dye Acid Red 88 adsorption by magnetic $ZnFe_2O_4$ spinel ferrite nanoparticles. *Colloid Interface Sci.*, **398**, 152-160.

[6]. L. Wang, J. Li, Y. Wang, L. Zhao, Q. Jiang, (2012). Adsorption capability for Congo red on nanocrystalline MFe_2O_4 (M = Mn, Fe, Co, Ni) spinel ferrites. *Chem. Eng. J.*, **181-182**, 72-79.

[7]. Y. Wang, D. Tian, W. Chu, M. Li, X. Lu, (2019). Nanoscaled magnetic $CuFe_2O_4$ as an activator of peroxymonosulfate for the degradation of antibiotics Norfloxacin. *Sep. Purif. Technol.*, **212**, 536-544.

[8]. K. Karthik, S. Dhanuskodi, C. Gobinath, S. Prabukumar, S. Sivaramakrishnan, (2017). Photocatalytic and antibacterial activities of hydrothermally prepared CdO nanoparticles. *Mater. Sci. Mater. Electron*, **28(15)**, 11420-11429. [9]. T.H. Shin, Y. Choi, S. Kim, J. Cheon, (2015). Recent advances in magnetic nanoparticlebased multi-modal imaging. *Chem. Soc. Rev.*, **44(14)**, 4501-4516.

[10]. C.S.S.R. Kumar, F. Mohammad, (2011). Magnetic nanomaterials for hyperthermia-based therapy and controlled drug delivery. Adv. *Drug Deliv. Rev.*, **63(9)**, 789-808.

11]. S. Laurent, S. Dutz, U.O. H¨ afeli, M. Mahmoudi, (2011). Magnetic fluid hyperthermia: focus on superparamagnetic iron oxide nanoparticles. *Adv. Colloid Interface Sci.*, **166(1-2)**, 8-23.

[12]. F. Valente, L. Astolfi, E. Simoni, S. Danti, V. Franceschini, M. Chicca, A. Martini, (2017. Nanoparticle drug

delivery systems for inner ear therapy: an overview. *Drug Deliv. Sci. Technol.*, **39**, 28-35.

[13]. H. Guo, W. Chen, X. Sun, Y.N. Liu, J. Li, J. Wang, (2015). Theranostic magnetoliposomes coated by carboxymethyl dextran with controlled release by low-frequency alternating magnetic field. *Carbohydr. Polym.*, **118**, 209-217.

[14]. W. Chen, Y. Zhou, J. Lu, X. Huang, W. Wu, C. Lin, Q. Wang, (2016). Effects of Li^+ substitution on the structural and magnetic properties of $Co_{0.5}Mn_{0.5}Fe_2O_4$ particles. *Ceram. Int.*, **42(1)**, 1114-1121.

[15]. S. Chandra, M.D. Patel, H. Lang, D. Bahadur, (2015). Dendrimer-functionalized magnetic nanoparticles: a new electrode material for electrochemical energy storage devices. *Journal of Power Sources*, **280**, 217-226.

[16]. R. Ahmad, I. Hussain Gul, M. Zarrar, H. Anwar, M.B. Khan Niazi, A. Khan, (2016). Improved electrical properties of cadmium substituted cobalt ferrites nanoparticles for microwave application. *Magn. Magn. Mater.*, **405**, 28-35.

[17]. M.J. Branislava, L.V.P. Vesna, N.V. Đorđe, V.R. Ljubinka, (2011). Arsenic removal from water using low-cost adsorbents - a comparative study. *J. Serb. Chem. Soc.*, **76(10)**, 1437-1452.

[18]. World Health Organization, (2008). Guidelines for Drinking-water Quality, WHO Press, Third Edition Incorporating The First And Second Addenda.

[19]. A.H. Khan, S.B. Rasul, A. Munir, M. Habibuddowla, M. Alauddin, S.S. Newaz, A. Hussan, (2000). Appraisal of a simple arsenic removal method for groundwater of Bangladesh. *J. Environ. Sci. Health*, **35(7)**, 1021-1041.

[20]. WHO/UNICEFF, (2015). Meeting the fundamental need for water, sanitation and hygiene services in health care facilities, Global meeting held Madrid.

[21]. L.V. Rajaković, (1986). Faculty of Technology and Metallurgy. PhD Thesis, University of Belgrade, Belgrade.

[22]. K.J. Chakresh, A. Imran, (2000). Arsenic: occurrence, toxicity and speciation techniques, *Water Reseach*, **34(17)**, 4304-4312.

[23]. D. Wolfgang, S. Reiner, J. Martin, (1995). Oxidation of arsenate (III) with manganese oxides in water treatment. *Water Research*, **29(1)**, 297-305.

[24]. Giménez J., Martínez M., dePablo J., Rovira M., Duro L.G, (2007). Arsenic sorption onto natural hematite, magnetite, and goethite. *Journal of Hazardous Materials*, **141**, 575-580.

[25]. Moore J.N., Walker J.R., Hayes T.H., (1990). Reaction scheme for the oxidation of As (III) to arsenic (V) by birnessite. *Clays Clay Miner*, **38**, 549-555.

[26]. Tokunaga S., Wasay S. A., Park S. W, (1997). Removal of arsenic (V) ion from aqueous solutions by Lanthanum compounds. *Water Science Technology*, **35(7)**, 71-78.

[27]. Luu Minh Dai, Nguyen Thi To Loan, Dao Ngoc Nhiem, Vu The Ninh, (2008). Synthesis of MnO_2 nano scale by the gel combustion and studying the possibility of using MnO_2 nano scale to adsorb arsenic. *Vietnam Journal of chemistry*, **46(2A)**, 43-49.

[28]. L. Jriuan, V.P.M Kurikka, M. Shafi, U. Abraham, L. Katja, Y.N. Loh, C.M. Hui C., V. Thomas, E. Claude, C.L. Dave, (2004). Mixed iron-manganese oxide nanoparticles. *J. Phys. Chem. B.*, **108(39)**, 14876-14883.

[29]. G.L. Jae, H.K. Jung, P.C. Kwang, (2006). Crystallographic and Magnetic Properties of Zn-Mn Ferrite. *Journal of the Korean Physical Society*, **49(2)**, 604-607.

[30]. D. Tripathy, A.O. Adeyeye, C.B. Boothroyd, S. Shannigrahi, (2008). Microstructure and magnetotransport properties of Cu doped Fe_3O_4 films.

Journal of Appied Physics, **103**, 07F701-07F703.

[31]. J. Giri, P. Pradhan, V. Somani, (2008). Synthesis and characterizations of water-based ferrofluids of substituted ferrites [$Fe_{1-x}B_xFe_2O_4$, B = Mn, Co (x = 0-1)] for biomedical applications. *Journal of Magnetism and Magnetic Materials*, **320**, 724-730.

[32]. S. Zhang, H. Niu, Y. Cai, (2010). Arsenite and arsenate adsorption on co-precipitated bimetal oxide magnetic nanomaterials: $MnFe_2O_4$ and $CoFe_2O_4$. *Chemical Engineering Journal*, **158**, 599-607.

[33]. Pham Thi Lan Huong, Nguyen Tu, (2018). Functional manganese ferrite/graphene oxide nanocomposites: effects of graphene oxide on the adsorption mechanisms of organic MB dye and inorganic As(V) ions from aqueous solution, *Royal Society of Chemistry Advances*, **8**, 12376-12389.

[34]. J. Hu, I.M.C. Lo, G.H. Chen, (2007). Comparative study of various magnetic nanoparticles for Cr(VI) removal. *Separation and Purification Technology*, **56**, 249-256.

[35]. Vu The Ninh, Dinh Xuan Loc, Tran Anh Tai, (2020). Study on synthesis and characterization of nano scale spinel $Mn_{0.5}Fe_{2.5}O_4$ by microemulsion method. *Vietnam Journal of Catalysis and Adsorption*, **9(4)**, 29-35.